Frontiers in Bioscience Landmark

Front. Biosci. (Landmark Ed) **2022**; 27(9): 273
https://doi.org/10.31083/j.fbl2709273

Original Research

Effect of Direct Current Electric Fields on Cone Like Retinal Photoreceptor Cells

Juliana Guerra-Hühne[1,2,†], Sharanya Bola[1,†], Daniela Calzia[3], Dimitra Alexopoulou[4], Richard H.W. Funk[1,*], Sergio S. Mühlen[2,‡], Cora Roehlecke[1]

[1]Department of Anatomy, Medical Theoretical Center, TU-Dresden, 01069 Dresden, Germany
[2]Center and Department of Biomedical Engineering/Unicamp, 13083-872 Campinas-SP, Brazil
[3]Department of Pharmacy-DIFAR, Biochemistry and Physiology Lab, University of Genoa, Via le Benedetto 16126 Genova, Italy
[4]Deep Sequencing Group SFB 655, Biotechnology Center, TU-Dresden, 01069 Dresden, Germany
*Correspondence: richard.funk@tu-dresden.de (Richard H.W. Funk)
[†]These authors contributed equally.
[‡]Dead author.

Academic Editor: Graham Pawelec
Submitted: 2 July 2022 Revised: 7 September 2022 Accepted: 19 September 2022 Published: 29 September 2022

Abstract

Introduction: Studies show that electric fields are used as therapy during nerve and tissue injuries along with trans-retinal stimulation. However, cellular and molecular changes induced by such treatments remain largely unknown especially in retinal photoreceptor cells. *In vitro* studies show that direct current electric fields (dcEF) were known to influence cell division, polarity, shape, and motility. Here we could characterize for the first time the reactions of 661W, a retinal cone photoreceptor especially regarding organelle polarization, membrane polarization of mitochondria, O_2 consumption, ATP/ADP ratio and gene expression. **Methods**: The 661W cells were stimulated with a constant dcEF of field strength 5 V/cm during 30 min or 5 h depending on the parameters studied. **Results**: In response to dcEF, the cells aligned perpendicular to the field by forming a leading edge with extended membrane protrusions towards the cathode. Using immunofluorescence and live cell imaging, we show that the cell membrane depolarized at the cathodal side. The microtubules spread into the direction of migration. Also, the microtubule organization center re-oriented into this direction. Concomitantly with the microtubules, actin filaments reorganized in an asymmetrical fashion mainly at the cathodal side. The Golgi apparatus, which is involved in many steps of actin synthesis, moved to the cathodal side. In the last 2 h of the 5 h experiment, microtubules positioned themselves at the rear (anodal side), like the nucleus. The averaged displacement of the whole cells under dcEF was 155% of control for 3 V/cm and 235% for 5 V/cm. The average speed increased by 142% and 243% respectively. Inside the cells mitochondria moved to the cathodal side, where the energy consuming producing processes take place. In this line, we measured an increase in ATP production and O_2 consumption. Mitochondrial calcium was found more on the anodal side, at the site of the nucleus with its calcium delivering endoplasmic reticulum. In addition, oxymetry studies reveal an increased ATP synthesis by 115.2% and oxygen consumption by 113.3% 3 h after dcEF stimulation. An analysis of differentially expressed genes by RNA sequencing revealed an upregulation of genes involved in cellular movement, cell to cell and intracellular signaling, molecular transport, assembly and organization. **Conclusions**: The mechanisms found can enhance our understanding regarding the beneficial effects of EF treatment in retinal diseases.

Keywords: cell migration; polarization; retinal photoreceptor; cytoskeleton; O_2 consumption; ATP production; electric fields

1. Introduction

Photoreceptor dystrophies and degenerative diseases of the retina are major causes of blindness worldwide, ranging till 5–14% in age-related macular degeneration [1]. In recent studies, electric fields (EF, e.g., via transcorneal electric stimulation - TCES) have been successfully applied to treat such retinal diseases [2–6] as well of degenerative diseases of the optic nerve [7,8].

Regarding pathophysiology, it could be demonstrated that TCES treatment inhibits the expression of proinflammatory cytokines, while upregulating the expression of IL-10, protected retinal cell survival through downregulation of NF-kappaB signaling pathway or at least partly via anti-inflammation mechanism and attenuating microglial activation [9]. In general, electric fields (endogenous as well as externally applied) play an important role for directing cell migration, for wound healing, development, and regeneration. In cultures, applied direct current electric fields (EF) influence cell division, polarity, shape, and motility. As an example of retinal cells, EF direct retinal ganglion cell axon growth *in vitro* [8]. Also, neural stem cells could be guided by EF [10]. This electrical signal overrides all other biochemical signaling in the migration pathway, offering a tool in brain stem cell therapies [11].

In general, cell migration is a complex process that involves membrane protrusion, adhesion and retraction [12, 13]. The forces driving the process of migration in various physiological and pathological conditions are dependent on

Copyright: © 2022 The Author(s). Published by IMR Press.
This is an open access article under the CC BY 4.0 license.

Publisher's Note: IMR Press stays neutral with regard to jurisdictional claims in published maps and institutional affiliations.

chemical signals and extracellular environment. Apart from other cues like chemical gradients and mechanical forces which induce cell migration, the significance of endogenous EF as candidate signals for numerous physiological processes has been confirmed repeatedly [14,15].

Endogenous electric signals play significant role in various biological processes such as development, wound healing, and regeneration [16–18]. Endogenous ionic currents detected by vibrating probe experiments in developing embryos [19,20] amputated limbs [21] and at wound sites [17] were in the same order of magnitude as currents produced by electric field strengths required to induce directional cell migration *in vitro* [22,23].

Various studies confirm that numerous cell types migrate towards cathode or anode in the presence of EF through a process known as electrotaxis or galvanotaxis [24–29]. Cellular responses to EF either at trailing or leading edge, ultimately polarize the cells with asymmetric distribution of signaling molecules and redistribution of focal adhesions to induce persistent directional migration [17,24,26,30]. Those cellular activities like polarization and persistent directional migration might involve multiple signaling pathways such as focal adhesion kinase [31] that orchestrate with each other due to asymmetric localization of cell membrane receptors which initiate signal transduction to downstream effectors upon EF stimulation [32–35]. However, directed migration and polarization requires cytoskeletal reorganization and its interaction with ion transporters along with variety of intracellular response [36,37]. Yet the mechanism of how these electrical signals are interpreted by the cell remains unclear, but they should involve asymmetric ionic flow through voltage gated channels [38].

In the present study, we looked for basic mechanisms of EF effects on photoreceptor-like cell polarity and polarization of intracellular structures. Using a well-established migration assay, photoreceptor cone-like 661W mouse retina cells. This cell line was taken because of positive clinical results after electrical stimulation in retinal degenerative diseases (see above) and because retinal photoreceptor cells must orient within the eye exactly in the direction of the light beam. In addition, these cells exhibit cellular and biochemical characteristics of cone photoreceptor cells [39]. To achieve the objectives and parameters mentioned above, we conducted a series of different experiments with different dcEF intensities (of physiological levels) and times of exposition using a steady electric field during the whole stimulation period. Cells were exposed to dcEF strength of 3 V/cm and 5 V/cm, consistent with physiological dcEF and also with those applied in similar studies in other cell types [35,36]. We used dcEF because in most cases of endogenous wound healing steady (direct) currents are involved [13–16]. Also, in neuroprotection studies of the eye often dcEF were applied [7].

Using immunofluorescence techniques, we have investigated repositioning of important organelles and cytoskeletal proteins following stimulation. Furthermore, we investigated local changes in plasma and mitochondrial membrane potentials using ion reporter dyes in the presence and absence of an applied EF.

In response to the directional stimulus dcEF, cells extended membrane protrusions and formed a leading edge towards the cathode becoming elongated perpendicular to the EF. Directional migration occurred towards the cathode (averaged displacement 155% of control for 3 V/cm and 235% for 5 V/cm; average speed increased by 142% and 243% respectively).

Cytoskeleton proteins and organelles moved asymmetrically in the cells. Actin cytoskeleton, microtubule organizing center (MTOC) and Golgi apparatus (GA) were reoriented in the direction of the leading edge, while microtubules (MTs) accumulated in the rear edge of the cells. The nucleus was translocated to the rear edge. After EF exposure, both plasma and mitochondrial membranes were depolarized, especially at the cathodal side of the cells. Upon exposure to EF, there is increase in mitochondrial respiration and ATP synthesis, especially under prolonged stimulation (absolute and percentage data are given in chapter "results").

Because an exact positioning of photoreceptors is a key issue in retinal architecture, our study can give hints to achieve this goal by directed EF. Here, for the first time the migration, rearrangement of the inner architecture of such retinal cells and the energetic expense of such changes, could be monitored in single cells.

2. Materials and Methods

2.1 661W Cell Culture

We used an immortalized mouse retinal cell line 661W, kindly provided by Dr. Muayyad Al-Ubaidi (Department of Cell Biology, University of Oklahoma Health Sciences Center, USA). The cells were cultured in Dulbecco's modified Eagle Medium (DMEM) (Gibco, Germany) supplemented with 10% fetal calf serum (FCS) (Biochrom, Germany). Cultures were maintained at 37 °C in humidified air and 5% CO_2 and sub-cultured every third day. Based on flow cytometry or microscopy experiments, 150 μL of cell suspension with density of 5×10^4–1×10^5 cells/mL were seeded into the channels of Ibidi μ-slide (Ibidi, Munich, Germany).

2.2 Experimental Set Up

The setup for EF stimulation is shown in Figs. 1,2. Cells were seeded with density of 5×10^4–1×10^5 cells/ml in μ-slides a day before the experiment. The slides were placed on the stage of an inverted microscope. Just prior to start of experiment, fresh medium was added to the channel of the μ-Slide so that any cell remnants get washed off. A constant source of direct current (BioRad, Germany) was applied to the cells via two platinum electrodes (0.2 mm in diameter, Agar Scientific, Essex/UK), which

were immersed in 0.9% NaCl filled beakers. On the other side, the platinum electrodes (electrode gap 50 mm) were connected to the medium reservoirs of the μ-Slide chamber by two 20 cm-long agar bridges (2% agar in PBS). HBSS and cell culture media was used for the ion imaging and migration assay, respectively. Platinum electrodes and agar-bridges were used to avoid diffusion of the electrode products into the culture. A voltmeter (Voltcraft® Meßtechnik, Germany) was used to measure the thresholds of current throughout the experiment to ensure that the EF strength was kept constant on the chosen value (3 or 5 V/cm) (Figs. 1,2). The cells were exposed for 5 h to EF of 3 V/cm or 5 V/cm. In our pilot experiments, the cells started to dye at intensities of 8 V/cm. Intensities of 3 and 5 V/cm and duration of dcEF application of 5 h proved to be optimal for reorientation and migration studies. For studies of cell metabolism and of respiratory parameters 30 min and 3 V/cm were used.

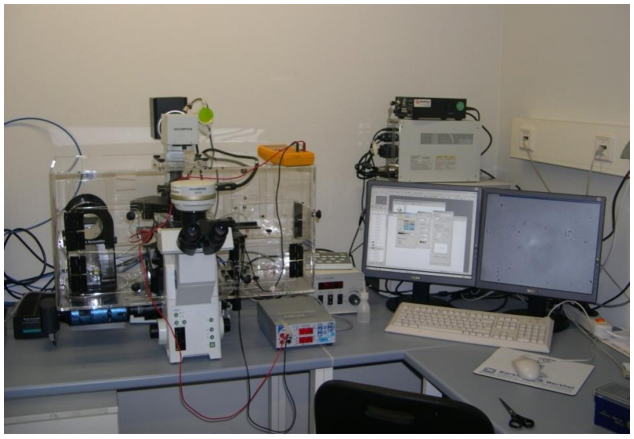

Fig. 1. Setup for life cell imaging and computerized data acquisition. Cells are placed within the medium reservoir (Ibidi μ-slide) under the microscope. The big transparent box (1) around the microscope dish renders full incubator conditions by measuring and controlling humidity and temperature. The power supply (2) is connected to the medium chamber (see Fig. 2).

To determine whether the physiological dcEF is causing cellular death or not, we evaluated the viability of the cells after the exposure to EF. We used the viability/cytotoxicity assay (LIVE/DEAD® Molecular Probes) to determine the death rate of cells 5 h after exposure to dcEF. The assay was conducted in each different group studied: control, 30 min and 5 h 3 V/cm, 5 h 5 V/cm, 5 h 8 V/cm. The viability was checked directly after dcEF and 5 h after the dcEF. Death rate was 5.4% for 3 V/cm and 6% for 5 V/cm (N = 5, Ncell = 500) at 5 h of exposure. In controls (no dcEF) 4% of dead cells were found. Further control experiments after 5 h showed that in mitochondria the red/green ratio of the JC1 was the same as in the stimulation period, using flow cytometry.

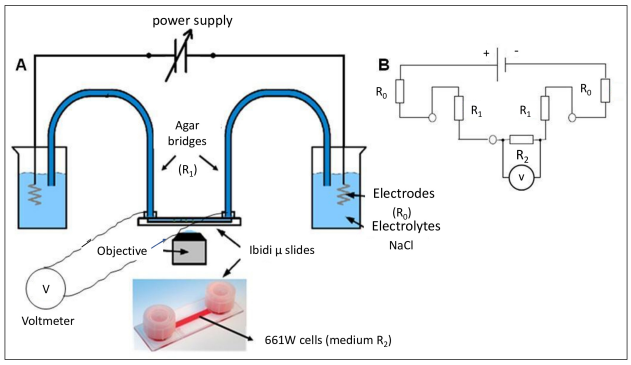

Fig. 2. Schematic drawing of the experimental set up used in the migration assay. (A) Consisting of a power supply, 2 beakers with saline solution (0.9% NaCl), 2 agar-bridges (2% agar), vital microscope (Olympus IX81) and cultivated cells in μ-slides. (B) Simplified diagram of the respective electrical circuit formed by the electrodes (R0), agar bridges (R1) and medium (R2).

For plasma and mitochondrial analysis, control cells were divided into two groups: (1) untreated control cells (2) positive control cells (treated with Gramicidin and CCCP for plasma and mitochondrial membrane potential, respectively). For cell motility experiments, migration was monitored via an Olympus IX81 (Olympus, Hamburg/Germany) inverted microscope and the acquisition of images was controlled by Xcellence software (Olympus, Germany, version 1.2) (Fig. 1).

2.3 Plasma Membrane Potential

For microscopy experiments, 2 mL of 0.1 μM $DiBAC_4$ (3) (Invitrogen, Germany) in PBS solution was added to the slides and the cells were incubated for 5 min at 37 °C, 5% CO_2. For flow cytometry, cells were trypsinized, centrifuged and counted and then, 1 mL of 0.5 μM dye solution was added to the cells. For gramicidin-treated cells, first Gramicidin (5 μM) diluted in high KCl HBSS buffer was added to the cells (10 min) and afterwards, $DiBAC_4$ (3) with high KCl HBSS buffer was added.

2.4 Mitochondrial Membrane Potential

For microscopy, 1.5 μM JC-1 (Molecular Probes, Germany) dye was diluted in 1 mL of basal medium and centrifuged at 21,000 rpm, 4 °C for 5 min before being mixed and added to the cells. The cells were then incubated for 15–20 min at 37 °C, 5% CO_2. For CCCP-treated cells, 100 μM CCCP diluted in 1 mL buffer was added to the cells and then, JC-1 solution was added. In the flow cytometry experiments, the same procedure was used for staining the cells. Cells were trypsinized, centrifuged and counted after staining.

2.5 Immunofluorescence

Following EF treatment, cells were fixed with 4% paraformaldehyde (5 min), permeabilized (6 min in 10

μg/mL Digitonin in PBS) and blocked with 2% BSA (w/v) in PBS for 15 min at RT. The cells were then incubated with primary antibodies-rabbit polyclonal anti γ-tubulin (1:250, Abcam, Germany), mouse monoclonal anti β-cop (1:150, Sigma Aldrich, Germany) and rabbit polyclonal anti β-III-tubulin (1:700, Abcam, Germany) for overnight at 4 °C. Cells were washed with PBS and incubated with secondary antibodies [FITC Goat anti rabbit (1:1500), Texas Red Goat anti mouse (1:800), FITC Goat anti rabbit (1:2000), Jackson ImmunoResearch laboratories, USA] for 1 h in dark at RT. Nuclei were stained with DAPI (1:50, Sigma-Aldrich, Germany) and 2.5% DABKO (Sigma Aldrich, Germany) was used as mounting solution.

2.6 mRNA Isolation and Sequencing

For RNA isolation, EF stimulated 661W cells and control cells in Ibidi slides were trypsinized and centrifuged at 150 g for 5 min Supernatants were aspirated and later total RNA isolation was done according to manufacturer's instructions (Qiagen, Germany). The RNA integrity was checked using 2100 bioanalyzer. mRNA was isolated from 1 μg total RNA by poly-dT enrichment using the NEBNext Poly (A) mRNA Magnetic Isolation Module according to the manufacturer's instructions. After chemical fragmentation the samples were directly subjected to strand specific RNA-Seq library preparation (Ultra Directional RNA Library Prep, NEB). For adapter ligation custom adaptors were used (Adaptor-Oligo 1: 5′-ACA-CTC-TTT-CCC-TAC-ACG-ACG-CTC-TTC-CGA-TCT-3′, Adaptor-Oligo 2: 5′-P-GAT-CGG-AAG-AGC-ACA-CGT-CTG-AAC-TCC-AGT-CAC-3′). After ligation, adapters were depleted by SpriBead bead purification (Beckman Coulter). Sample indexing was done in the following PCR enrichment (15 cycles). For Illumina flowcell production, samples were equimolarly pooled and distributed on all lanes used for 75 bp single end sequencing on Illumina HiSeq 2500.

2.7 Oxygen Consumption Measurements

An amperometric electrode (Unisense-Micros respiration, Unisense A/S, Denmark) was used to measure the oxygen consumption. The experiment was performed in a closed chamber at 23 °C. For each experiment, around 2×10^5 cells (0.04 mg) were permeabilized with 0.03 mg/mL digitonin for 1 min, centrifuged for 9 min at 1000 rpm and resuspended in: 137 mM NaCl, 0.7 mM NaH_2PO_4, 5 mM KCl, and 25 mM Tris HCl (pH 7.4). The same medium was used in the oximetric experiments. 10 mM pyruvate and 5 mM malate was added to the sample to stimulate OXPHOS machinery. To study if OXPHOS is coupled, 0.1 mM ADP was added 2 min after oxidative substrate addition.

2.8 ATP Synthesis Assay

ATP formation from ADP and inorganic phosphate (Pi) in 661W cells was measured by the luciferin/luciferase chemiluminescent method (Roche Applied Science), as described previously [38]. Cells (5 μg protein) were permeabilized with 0.03 mg/mL digitonin for 1 min, centrifuged for 9 min at 1000 rpm and resuspended in 50 mM Tris HCl (pH 7.4), 5 mM KCl, 1 mM EGTA, 5 mM $MgCl_2$, 0.6 mM ouabain, 5 mM KH_2PO_4, 5 mM pyruvate and 2.5 mM malate and ampicillin (25 μg/mL). ATP synthesis was induced by adding 0.3 mM ADP.

2.9 β-actin and Mitochondrial Calcium Transfections

0.2 μg of each pAcGFP1-Actin (Clontech Laboratories, USA) and mito-GcaMP2 (Dr. Wang, Peking University) plasmids were used to transfect the cells for β-actin and mitochondrial calcium ($[Ca^{2+}]_{mito}$). Cells were transfected using Lipofectamine 2000 (Invitrogen, Germany) according to manufacturer's protocol. 4 h after transfection, complete growth medium was added and left undisturbed until the next morning.

2.10 Analysis of Data

2.10.1 Cell Motility

Images were taken every 1 min during 5 h. An average number of 125 cells were scored for each condition (n = 10). The cell movement during application of EF, to cathode (–) or anode (+), was tracked using the Olympus imaging software Cell^R. Manual settings were used for cell tracking. In order to quantify the cell speed (μm/h), directedness (°) and net linear displacement (μm), time-lapse DIC videos were processed in the detecting program, TrackIT. Polar diagrams were created using PSI-Plot (version 9.5, Poly Software International, New York/USA).

2.10.2 Fluorescence

To quantify polarization, the cell body from 661W cells was divided into a cathodal half and an anodal half by a line perpendicular to the applied EF and through the center of the cell. The percentage of fluorescence intensity in each half of the cells was calculated considering the total fluorescence exhibited in the cell by using ImageJ software (Open source software; National Institutes of Health, Bethesda, MD, USA). This criterion was used for scoring polarization of Golgi apparatus (GA), microtubules organizing center (MTOC), microtubules (MTs), actin and nucleus and also for the accumulation of the dyes for plasma and mitochondria membrane potentials. All measurements were made considering reduction of background and normalization by the area. Flow cytometry analysis was done using CellQuest software (Version 5.2.1 BD Biosciences, San Jose, CA, USA).

2.10.3 Bioinformatics

Alignment of the short reads to the mm10 transcriptome was performed with GSNAP [40] and a table of read counts per gene was created based on the overlap of the uniquely mapped reads with the Ensembl Genes annotation

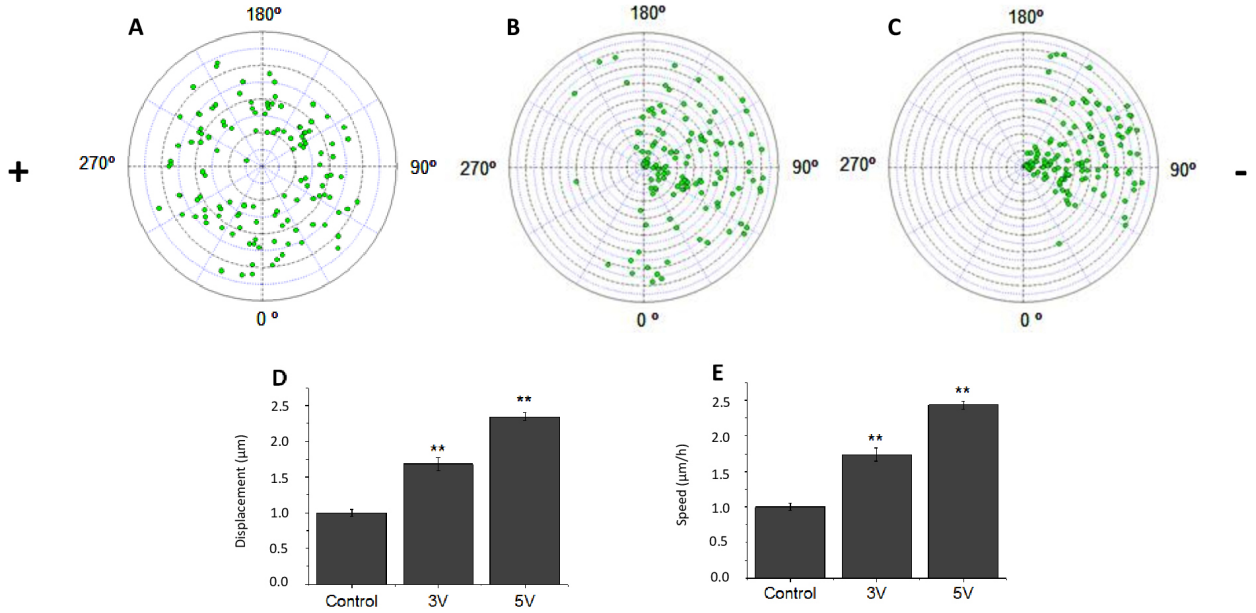

Fig. 3. Electrotaxis of 661W cells in the presence and absence of EF. (A) Polar plot shows random cell migration in the absence of EF. (B) Polar plot shows the cathodal migration of the cells at 3 V/cm EF. (C) Polar plot shows cathode directed migration of cells at 5 V/cm EF. (D) Averaged displacement of cells and (E) Speed of the cells. Controls show smaller displacement, while EF stimulated cells show significant increase in cell displacement and speed. Signs (+/–) show the polarity of the electric field. n = 10, ** $p < 0.01$. The values were normalized by control (control = 1) and means ± S.E.M. were plotted.

v. 81 (European Molecular Biology Laboratory's European Bioinformatics Institute, Hinxton, United Kingdom) (July 2015) for mm10, using feature Counts (v. 1.4.6) [41]. The raw read counts were normalized based on the library size and the testing for differential expression between the different cell treatments was performed with the DESeq2 R package (v.1.8.1) [42]. Based on the normalized gene expression level, sample to sample Euclidean distance as well as Pearson's correlation coefficient (r) were computed to explore correlation between biological replicates and different libraries. Differential expression was tested by fitting the count data to the negative binomial distribution. The p-values for the statistical significance of the fold change were adjusted for multiple testing with the Benjamini-Hochberg correction for controlling the false discovery rate [43]. Accepting a maximum of 10% false detections, this resulted in significantly upregulated and downregulated genes.

2.10.4 Statistics

Each set of data analyzed was previously tested for normality using the Lillie test on Matlab (version 9.3, Matlab is a program of MathWorks, Inc. Natick, MA, USA). The data was then normalized by the average of the control group. Statistics were calculated using ANOVA (normal data) and Kruskall-Wallis test (non-normal data). The considered α was 0.05 and a *Post hoc* analysis was performed using Bonferroni corrections. n is the number of independent experiments and n_{cell} is the number of cells from each group.

3. Results

3.1 Voltage Dependent Electric Field Guided Migration

We investigated the effects of direct current electric fields on migration of 661W cells. Cells were stimulated with different voltages (3 V/cm, 5 V/cm) and were monitored with time-lapse video imaging software for 5 h. The displacement of migrating cells at different conditions (control, EF 3 V/cm, EF 5 V/cm) was analyzed. The trajectory of cell migration is random in controls (no dcEF) (Fig. 3A); during EF stimulation (3 V/cm) (Fig. 3B) it is directed towards cathode, more directed with increased field strength (Fig. 3C). In absence of EF, cells migrated randomly with decreased displacement and migration velocity (Fig. 3D). Depending upon EF strengths, cells migrated more actively with significant increase in displacement and speed (Fig. 3D,E). In Fig. 3A–C, each dot represents a cell, and its relative position represents the distance travelled by cells from the center of the plot (coordinates 0, 0). The morphological changes of the cells at different time frames during 5 h duration was monitored in the presence and absence of EF (**Supplementary Fig. 1**). In an applied EF, cells facing the cathode exhibited protrusive activity and are strongly aligned perpendicularly to the field when compared to control cells which kept an amorphous form. Experiments reversing the polarity of the EF applied were done to verify the reliability of the directional response. Thus, upon reversing the field after 2.5 h, the cells responses were fully reversed (**Supplementary Video 1**).

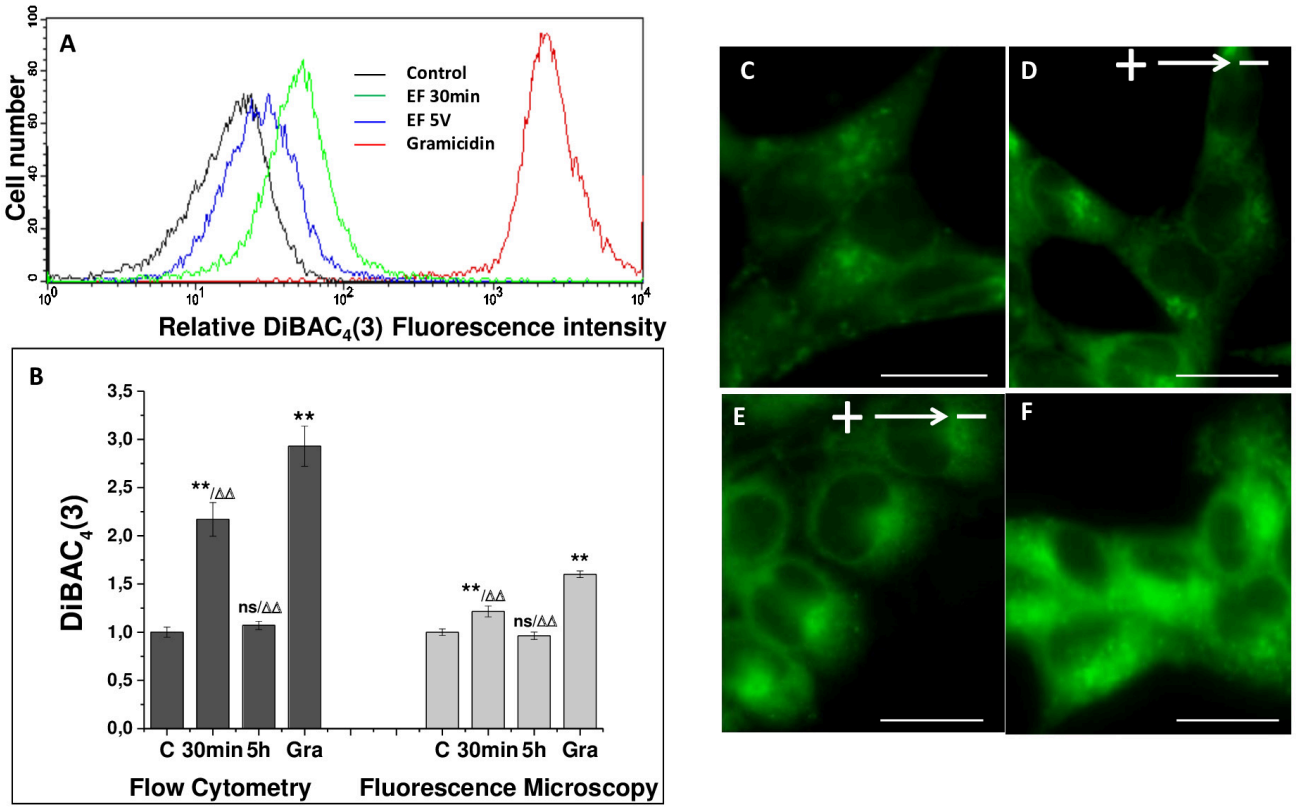

Fig. 4. Response of DiBAC$_4$ (3) to plasma membrane potential in 661W cells when stimulated with EF. Gramicidin which depolarizes the plasma membrane was used as a positive control. (A) Histogram shows representative change in fluorescence at different experimental conditions: control, EF (30 min), EF (5 h), and Gramicidin (B) Mean fluorescence intensity measured with flow cytometry and with ImageJ (microscopy). Values were normalized to control. (C–F) Fluorescent images of 661W cells showing the accumulation of dye during different treated conditions: (C) control, (D) 5 h 5 V/cm, (E) 30 min 5 V/cm, and (F) Gramicidin-treated cells. Signs (+/–) show the polarity of the electric field. n of experiments = 4, n of cells = 150,000 for flow cytometry and n = 4, n cells = 50 for fluorescence microscopy. ** $p < 0.01$ to control, $\Delta\Delta$ $p < 0.01$ to positive control, ns, not significant. Scale bar, 100 μm. Means $\pm$ S.E.M. were plotted.

3.2 EF Contributes to Time Dependent Changes of Plasma Membrane Potential

To monitor the changes of plasma membrane potential in the presence and absence of EF, we used plasma membrane specific-dye, DiBAC$_4$ (3). This dye is an anionic oxonal dye which increases in its fluorescence intensity upon membrane depolarization. Shortly after stimulation with 5 V/cm for 30 min and 5 h, 661W cells were loaded with DiBAC$_4$ (3) and the dynamic changes in the plasma membrane were measured by FACS (Fig. 4A) and fluorescence microscopy. Microscopy and cytometry analysis revealed that short-term stimulation (30 min) with EF caused significant increase in the fluorescence intensity, indicating a plasma membrane depolarization at the cathodal side. The increase in the fluorescence intensity profile was calculated from the baseline and was significantly higher in the dcEF-exposed cells (882.7 $\pm$ 32.3) than in the control cells (211.0 $\pm$ 14.1). However, long-term stimulation with EF (5 h) resulted in a decreased (not significant) depolarization of the membrane (Fig. 4B). By measuring the fluorescence intensity in the cells, we observed that the dye was accumulated in the cathodal side of 30 min EF exposed cells, while control cells as well as Gramicidin-treated cells showed random distribution of the dye indicating that the depolarization occurred preferentially in the cathodal side of the treated cells (Fig. 4C–F).

3.3 EF Contributes to Changes in Mitochondrial Membrane Potential

Control cells displayed fluorescence typical of mitochondria, corresponding to high potential. In contrast, positive control cells treated with CCCP presented an only green fluorescence pattern (Fig. 5A–E). In cytometric analysis, cells treated with EF exhibited mitochondrial membrane potential loss with 20% decreased fluorescence ratio in relation to control. There is an increased mitochondrial localization in the EF treated cells at the anodal side compared to the control cells where the distribution of mitochondria is random. In addition, the mitochondrial membrane potential is slightly higher (more red than green fluorescence) at the

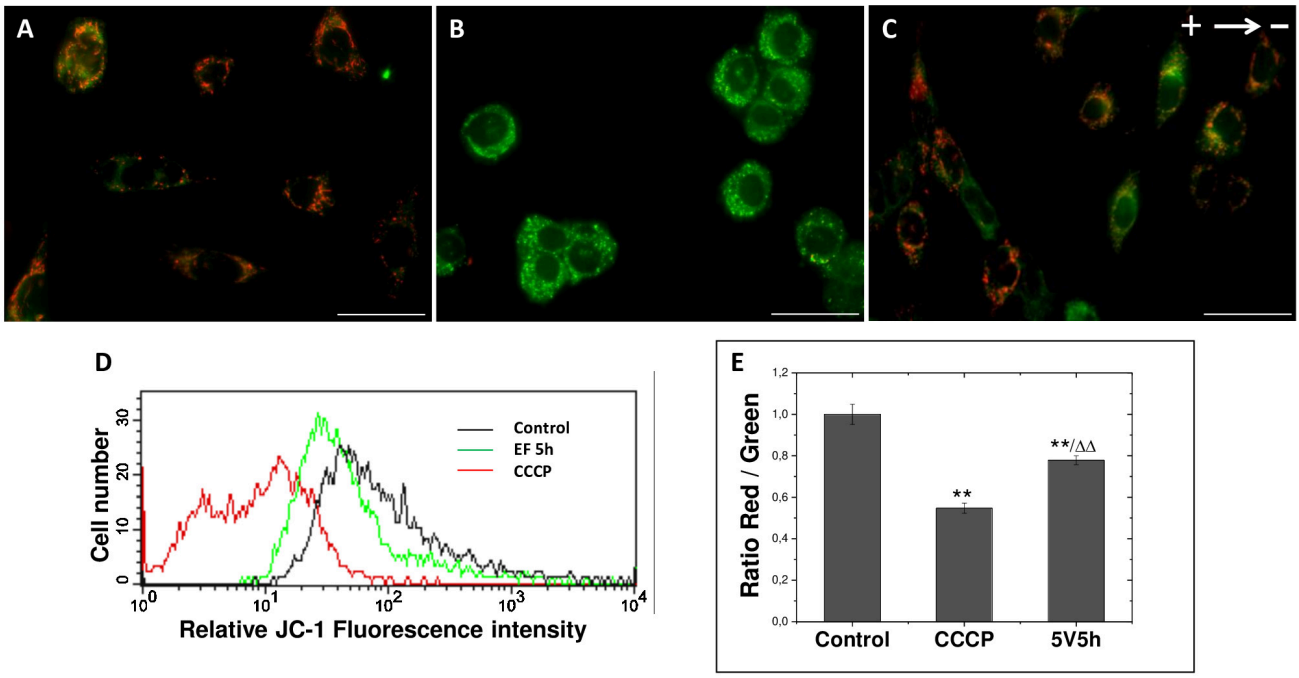

Fig. 5. Changes in mitochondrial membrane potential of 661W cells with EF stimulation. Mitochondrial membrane potential changes were monitored using JC-1 at different conditions. The ionophore CCCP was used to dissipate the mitochondrial membrane potential and to define the baseline for the analyses of mitochondrial potential. (A–C) Representative images of cells stained with JC-1 at different treated conditions: (A) control, (B) CCCP (positive control) and (C) EF (5 h 5 V/cm). Scale bar, 100 μm. Signs (+/–) show the polarity of the electric field. (D) Histogram shows representative change in fluorescence at different experimental conditions: control, EF (5 h), and CCCP treated (E) Ratio of red to green fluorescence was calculated as mitochondrial membrane potential. Quantitative analysis of the membrane potential measured at flow cytometry (light grey). n of experiments = 4, n of cells = 150,000 for flow cytometry. ** $p < 0.01$ in relation to control, $\Delta\Delta$ $p < 0.01$ in relation to the positive control**.** The values were normalized to control and means ± S.E.M. were plotted.

anodal side of the cell; also, the number of mitochondria is higher on this side. Furthermore, we analyzed the changes in mitochondrial calcium in the presence and absence of EF by transfecting the cells with mito-GcaMP2. We observed in the cells treated with EF an increased amount of mitochondrial calcium towards anodal side of the cells compared to control (**Supplementary Fig. 2**).

3.4 Increased ATP Synthesis and Oxygen Consumption upon EF Stimulation over Time

Upon exposure to EF, there is slight increase in mitochondrial consumption of oxygen in the presence of malate and pyruvate. As reported in Table 1 ADP stimulated oxygen consumption increased in time dependent manner in the presence of EF whereas in the presence of pyruvate/malate the consumption decreased after 1 h and then gradually increased after 3 h. Table 2 shows ATP synthesis by the same samples used in oxymetric analysis. ATP production by 661W cells is in the same order of magnitude that of control samples, when treated with EF for short time. Prolonged stimulation, however, leads to increased ATP synthesis.

Table 1. The respiration rates in 661W cells (0.04 mg total protein), after addition of 5 mM Pyruvate and 2.5 mM Malate and 0.3 mM ADP to stimulate oxygen consumption.

Samples	nmol O/min /mg protein	
	Pyruvate/malate	ADP
Control	42.6 ± 4.8	55.8 ± 6.2
EF (1 h)	38.4 ± 4.9	64.63 ± 7.5
EF (3 h)	48.3 ± 3.3	69.7 ± 5.7

Data are the mean ± SD of three experiments.

Table 2. ATP production by 661W in the presence of Pyruvate (5 mM) and Malate (2.5 mM). Activity is expressed as pmol ATP/min/mg of total protein.

Samples	pmol ATP produced/min/mg protein
Control	201.2 ± 20.5
EF (1 h)	207.5 ± 23.8
EF (3 h)	231.8 ± 23

Data are the mean ± SD of three experiments.

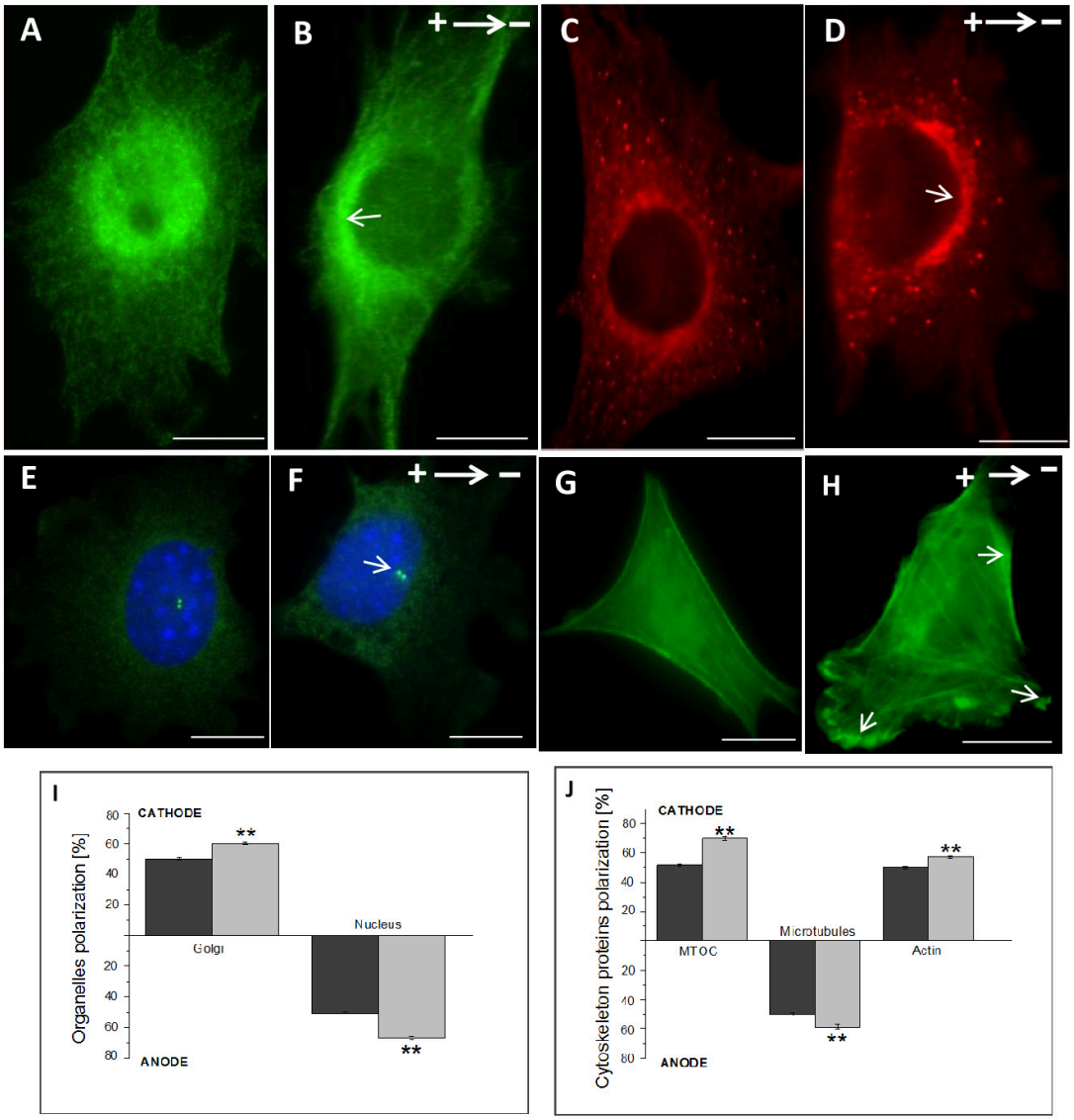

Fig. 6. EF induced organelle and cytoskeletal polarization in 661W cells. Immunostainings of microtubules (A,B), Golgi apparatus (C,D), MTOC and nucleus (E,F) and of actin transfected cells (G,H) showing morphological polarization in control and EF treated cells. Signs (+/–) show the polarity of the EF. Organelles became polarized after 5 V/cm 5 h EF exposure. (I) Percentage of organelles facing cathode (Golgi apparatus) or anode (nucleus) quadrants in cells stimulated with EF is significantly higher than in control cells (no EF). (J) Percentage of reoriented cytoskeletal proteins towards cathode (Actin, MTOC) and anode (Microtubules) quadrants is significantly higher in EF stimulated cells than in control cells. n = 4. ** $p < 0.01$ in relation to control. Scale bar, 20 μm.

3.5 Reorientation of Cytoskeletal Structures upon EF Stimulation

Polarization of organelles and cytoskeletal structures was random in absence of EF (Fig. 6A,C,E,G). However, after EF stimulation there is a significant redistribution of microtubules, Golgi, MTOC and actin towards cathode or anode (Fig. 6B,D,F,H). Microtubules which were reoriented in the direction of migration (cathodal side) initially were aligned perpendicular to the EF and positioned themselves at the rear (anodal side) after 5 h. (Fig. 6A,B). EF stimulation resulted in repositioning of 60.2% ± 0.9% of the Golgi complex towards cathode (Fig. 6C,D). MTOC reoriented towards cathodal side by 69.8% ± 1.2%, independent of microtubule accumulation. Upon EF Stimulation, the nuclei positioned themselves towards rear end by 66.8% ± 0.4% (Fig. 6E,F). Furthermore, the network of actin oriented along the field and reorganized in an asymmetrical fashion with an increased fluorescence at the cathodal side in the pAcGFP1-actin-transfected cells.

3.6 Differentially Regulated Genes Related to Biofunctions upon EF Stimulation

To understand the association of EF stimulation on cells, mRNA sequencing was performed. Our analysis shows that differential expression of genes due to EF govern

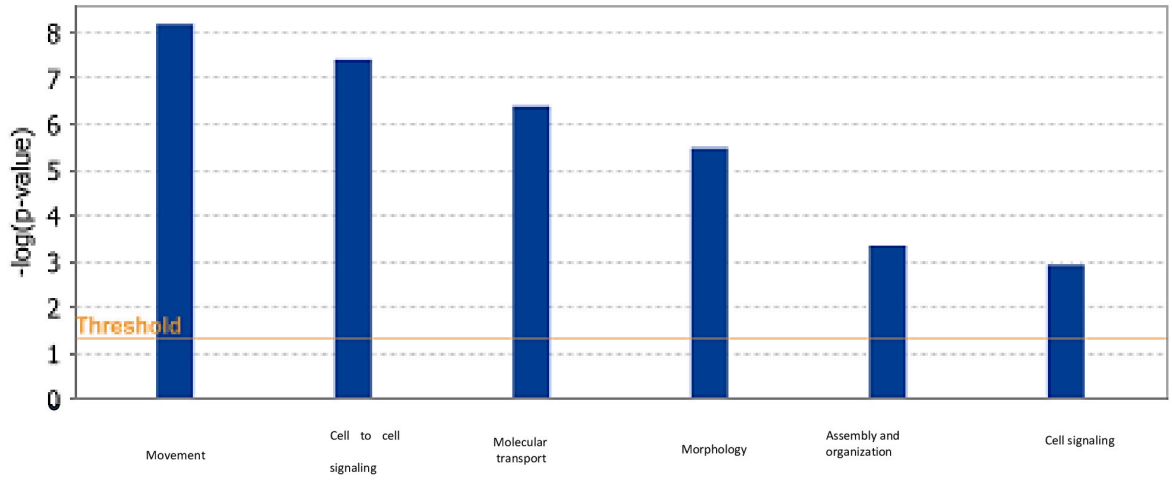

Fig. 7. The relative changes obtained through IPA analysis for bio-functions for the dataset of differentially expressed genes ($p < 0.001$) in EF stimulated cells. The threshold line in the bar chart represents p-values < 0.001.

several important molecular and cellular function. Of several functions, the major events altered were cellular movement, cell to cell signaling, molecular transport, morphology, assembly and organization, and cell signaling (Fig. 7). The respective genes involved in the functional networks are listed in **Supplementary Table 1**. Further studies are being carried out to study the effects of EF on different pathways in this cell line.

4. Discussion

Although the effect of EF has been previously shown in many different cell types [23,26,31,44,45], we could show here for the first-time direct EF effects on retinal photoreceptor-like cells. EF when applied had caused alterations in (i) migration, characterized by the active formation of lamellipodia which were clearly visible under light microscope (**Supplementary Fig. 1**). (ii) Directionality, which is cathodal oriented in this cell type (Fig. 3A–C) and, (iii) increased displacement and speed, which is dependent on voltage and time (Fig. 3D,E). The cells displayed positioned themselves perpendicular to the field with a wide lamellipodia at the leading edge and a small trailing edge that may be smooth (**Supplementary Fig. 1A–D**). Maximum alignment of 661W cells was reached within 5 h of stimulation at constant voltage.

In an EF, perpendicular cell positioning to the field occurs in order to minimize the stress due to the potential changes across the cell plasma membrane due to the constant voltage [46]. The transmembrane potential is affected by various electrical and geometrical properties of the cells such as membrane conductivity, shape and orientation (Fig. 4A–D). In our experiments, depolarization upon EF stimulation was characterized by an increased influx of dye initially which was later stabilized. This transient influx of dye accumulated at the cathodal side of the cells in the presence of EF compared with control cells where the dye accumulation was all over the cell (Fig. 4C–F). This inhomogeneity observed in the plasma membrane potential may be due to an imbalance in ion fluxes through activation of voltage gated ion channels [47]. However, in sum we observed a clear cathodal orientation of the depolarization.

Directed migration involves the initiation of cell polarity which is regulated by internal polarity effectors that promote the reorganization of cytoskeleton with well-defined front and rear ends [48]. Our findings indicate that actin, microtubules and the microtubule-organizing center (MTOC) are actively involved in the migratory response of 661W cells by being polarized to the cathodal or anodal side of the cells. In this work, we showed that actin selectively accumulated towards cathodal (leading) side of cells when stimulated by EF. In the absence of EF, the actin network was randomly distributed and extended in multiple directions wherein under certain circumstances the nucleus organizes actin structures [46]. From front to rear, actin-mediated forces sequentially promote cell protrusions, adhesion, contraction and retraction [49–53].

In our experiments, short term stimulation caused accumulation of microtubules in the cell front (cathodal side) and an increased accumulation towards anodal side of cells after long exposure times. Even though more microtubules grow towards the cell front, the density of microtubules close to the cell cortex is lower at the protruding front than in the retracting rear. This is probably caused by the speed of membrane protrusion exceeding that of microtubule polymerization together with the active rearward transport of microtubules by actin retrograde flow [54–56].

Our results also show reorientation of MTOC towards cathodal side. Microtubules and actin cytoskeleton can affect MTOC positioning through cytoskeletal linkers such as plectin that couple microtubules to myosin-powered actin retrograde flow [50,54–59]. Relative levels of the actin isoforms can regulate microtubule dy-

namics where β- and γ-actin filament networks have an opposite impact on microtubule dynamics and organization. Furthermore, microtubules can interact with the γ-actin cortical network directly via a +TIPs (microtubule plus-end/positive-end tracking proteins) protein complex [60]. Also, AMP-activated protein kinase (AMPK), an energy-sensing Ser/Thr protein kinase regulates microtubule dynamics through microtubule plus-end-tracking protein CLIP-170 phosphorylation [61]. The positioning of MTOC and Golgi towards the leading edge of the cell probably contributes to the targeted delivery of processed proteins along the microtubule towards the cells front [51,62]. We observed that Golgi positioned itself towards cathode as the positioning of the MTOC and its aster of microtubules mainly determines the positioning of the Golgi apparatus [63–66]. Besides, cathodal redistribution of Golgi and actin are interdependent, as inhibition of actin polymerization completely inhibited Golgi polarization, and inhibition of Golgi redistribution abrogated the polarization of cell morphology and F-actin [63]. These authors describe that in a strong EF, asymmetric Src and PI 3-kinase signaling as well as actin polymerization are essential for electric field-induced Golgi polarization and directional cell concomitant to changes in morphology and directional migration. Furthermore, the Golgi apparatus is a hub for a wide array of actin regulatory proteins [67]—e.g., the protein GOLPH3 links the Golgi to the actin cytoskeleton and is functionally important for directional cell migration [68].

We observed an increased mitochondrial calcium on anodal side of the cells after EF exposure and a high mitochondrial distribution at the anodal side (**Supplementary Fig. 2**). Increased mitochondrial calcium at the anodal side and decreased at the cathodal side could give rise to push-pull effects, causing net movement of cells towards the cathode. Here, it is well-known that mitochondria are involved in cellular calcium homeostasis [69–71]. Indeed, electric field-directed cell shape changes, displacement, and cytoskeletal reorganization were shown to be calcium dependent [72]. Regarding directed migration, increased localized intracellular calcium is involved together with various possible calcium pathways [73].

Our results suggest that increases in intracellular mitochondrial calcium may be a result of rapid changes in mitochondrial membrane potentials that surpass the membrane threshold due to applied electric fields. Furthermore, increased mitochondrial calcium drives an adaptive metabolic boost in stress situations like ER stress. Accordingly, blocking calcium transfer impaired a metabolic response, rendering cells more vulnerable to, e.g., ER stress [74]. Furthermore, calcium, which is released from ER by the inositol 1,4,5-triphosphate receptor is taken up by mitochondria where it is required for efficient oxygen consumption and ATP production [75].

In our experiments, we could directly monitor the increased energetic expense of concomitant changes in organelle cytoskeletal rearrangement and migration in the presence of EF. Here, we have found that ADP stimulated oxygen consumption increased in time dependent manner in the presence of EF whereas in the presence of pyruvate/malate the consumption decreased after 1 h and then gradually increased. We also showed that prolonged EF stimulation led to an increased ATP production. Regarding this, it is described that EF induced directed movement or migration in rigid media leads to a higher O_2 and ATP consumption [76].

Though EF activates the downstream signaling pathways through plasma membrane to recruit the components of cytoskeleton and polarity machinery, the exact signaling events between the external and internal cues remain unclear. Our present findings from sequencing will allow us to further study about directionality and polarization in the presence of EF. Fig. 7 and **Supplementary Table 1** show a few bio-functions and their possible candidate genes, differentially regulated in the presence of EF. Chemokine ligands and solute carrier transporters along with transmembrane reporters might activate the downstream signaling pathways for persistent directed migration and polarization in the EF stimulated cells, because chemokines and other genes mentioned are required in cell motility, assembly, and organization and signaling [77–79]. In this line, certain chemokines are known to induce calcium influx into the cells [80]. Also, the transporters expressed are involved in transport of cationic amino acids at the plasma membrane, phosphate linked antiporters at the ER, sodium independent, anionic amino acid transporters and also to maintain cellular iron ion homeostasis [81–83].

However, much more work has to be done to elucidate the detailed signaling mechanisms in all the here mentioned processes activated by EF.

5. Conclusions

Retinal 661W cells, are susceptible to EF like other retinal cells treated in *in vitro*, *in vivo* and in patients with transcorneal electrostimulation of the retina. Regarding polarization in the EF, we found the following events: directed migration towards the cathode with over two-fold increase in speed and displacement as well as significant depolarization of the plasma membrane at the leading edge of the cell (cathodal side). Then redistribution of microtubules into the direction of migration (cathodal side), initially aligned perpendicular to the EF. Also, the MTOC re-oriented into this direction. Concomitantly with the microtubules, actin oriented along the field and cell membrane and reorganized in an asymmetrical fashion with an increased fluorescence at the cathodal side. The cytoskeletal elements and the MTOC redistributed significantly from 50% (random) to 60–70% into the dcEF-induced direction. The Golgi apparatus, which is involved in many steps of actin synthesis, moved to the cathodal side by 65%. Later the microtubules positioned themselves at the rear (anodal side), like the nu-

cleus by 70% compared to the random 50% in controls without EF.

Interestingly, mitochondria and also the mitochondrial calcium moved to the anodal side, possibly because of energy consuming processes at the site of the nucleus and ER. We also measured an overall 115.2% increase in ATP production and 113.3% increase in O_2 consumption. The analysis of differentially expressed genes revealed a significant upregulation of gene expression involved in cellular movement, cell to cell signaling, molecular transport, assembly, and organization as well as cell signaling.

In sum, we could demonstrate that this cell type can easily be addressed by EF. The mechanisms found can enhance our understanding regarding beneficial effects of EF treatment in retinal diseases.

Author Contributions

JG-H. and SB performed most of the cell and molecular biologic experiments. DC did the experiments regarding metabolism. DA did the gene expression analysis. RHWF, SSM and CR designed the experiments and have written the manuscript together with JG-H and SB.

Ethics Approval and Consent to Participate

Not applicable.

Acknowledgment

Not applicable.

Funding

This research received no external funding.

Conflict of Interest

The authors declare no conflict of interest. RHWF is serving as one of the Editorial Board members and Guest Editors of this journal. We declare that RHWF had no involvement in the peer review of this article and has no access to information regarding its peer review. Full responsibility for the editorial process for this article was delegated to GP.

Supplementary Material

Supplementary material associated with this article can be found, in the online version, at https://doi.org/10.31083/j.fbl2709273.

References

[1] Flaxman SR, Bourne RRA, Resnikoff S, Ackland P, Braithwaite T, Cicinelli MV, *et al*. Global causes of blindness and distance vision impairment 1990–2020: a systematic review and meta-analysis. The Lancet Global Health. 2017; 5: e1221–e1234.

[2] Hu Y, Grodzki LM, Bartsch S, Bartsch U. Cell-Based Neuroprotection of Retinal Ganglion Cells in Animal Models of Optic Neuropathies. Biology. 2021; 10: 1181.

[3] Boia R, Ruzafa N, Aires ID, Pereiro X, Ambrósio AF, Vecino E, *et al*. Neuroprotective Strategies for Retinal Ganglion Cell Degeneration: Current Status and Challenges Ahead. International Journal of Molecular Sciences. 2020; 21: 2262.

[4] Sinim Kahraman N, Oner A. Effect of Transcorneal Electrical Stimulation on Patients with Retinitis Pigmentosa. Journal of Ocular Pharmacology and Therapeutics. 2020; 36: 609–617.

[5] Luu KY, Zhao M, Mannis MJ. The Use of Electrotherapeutics in Ophthalmology. American Journal of Ophthalmology. 2020; 211: 4–14.

[6] Kurimoto T, Ueda K, Mori S, Kamada S, Sakamoto M, Yamada-Nakanishi Y, *et al*. A Single-Arm, Prospective, Exploratory Study to Preliminarily Test Effectiveness and Safety of Skin Electrical Stimulation for Leber Hereditary Optic Neuropathy. Journal of Clinical Medicine. 2020; 9: 1359.

[7] Gokoffski KK, Peng M, Alas B, Lam P. Neuro-protection and neuro-regeneration of the optic nerve: recent advances and future directions. Current Opinion in Neurology. 2020; 33: 93–105.

[8] Fu L, Fung F, Koinzer S, Cheuk-Yin Lo A, Chan Y, So K, *et al*. Transcorneal Electrical Stimulation Inhibits Retinal Microglial Activation and Enhances Retinal Ganglion Cell Survival after Acute Ocular Hypertensive Injury. Translational Vision Science & Technology. 2018; 7: 2.

[9] Yao LL, Y. The Role of Direct Current Electric Field-Guided Stem Cell Migration in Neural Regeneration. Stem Cell Reviews and Reports. 2016; 12: 365–375.

[10] Feng J, Liu J, Zhang L, Jiang J, Russell M, Lyeth BG, *et al*. Electrical Guidance of Human Stem Cells in the Rat Brain. Stem Cell Reports. 2017; 9: 177–189.

[11] Pollard TD, Blanchoin L, Mullins RD. Molecular Mechanisms Controlling Actin Filament Dynamics in Nonmuscle Cells. Annual Review of Biophysics and Biomolecular Structure. 2000; 29: 545–576.

[12] Nobes CD, Hall A. Rho, rac and cdc42 GTPases: regulators of actin structures, cell adhesion and motility. Biochemical Society Transactions. 1995; 23: 456–459.

[13] Zhao M, Song B, Pu J, Wada T, Reid B, Tai G, *et al*. Electrical signals control wound healing through phosphatidylinositol-3-OH kinase-gamma and PTEN. Nature. 2006; 442: 457–460.

[14] Zhao M. Electrical fields in wound healing—an overriding signal that directs cell migration. Seminars in Cell & Developmental Biology. 2009; 20: 674–682.

[15] Song B, Zhao M, Forrester J, McCaig C. Nerve regeneration and wound healing are stimulated and directed by an endogenous electrical field in vivo. Journal of Cell Science. 2004; 117: 4681–4690.

[16] Reid B, Song B, McCaig CD, Zhao M. Wound healing in rat cornea: the role of electric currents. FASEB Journal. 2005; 19: 379–386.

[17] McCaig CD, Rajnicek AM, Song B, Zhao M. Controlling Cell Behavior Electrically: Current Views and Future Potential. Physiological Reviews. 2005; 85: 943–978.

[18] Reid B, Song B, Zhao M. Electric currents in Xenopus tadpole tail regeneration. Developmental Biology. 2009; 335: 198–207.

[19] Jaffe LF, Nuccitelli R. An Ultrasensitive Vibrating Probe for Measuring Steady Extracellular Currents. Journal of Cell Biology. 1974; 63: 614–628.

[20] Jaffe LF, Stern CD. Strong Electrical Currents Leave the Primitive Streak of Chick Embryos. Science. 1979; 206: 569–571.

[21] Borgens RB, Vanable JW, Jaffe LF. Bioelectricity and regeneration: large currents leave the stumps of regenerating newt limbs. Proceedings of the National Academy of Sciences. 1977; 74: 4528–4532.

[22] Robinson KR. The responses of cells to electrical fields: a review. Journal of Cell Biology. 1985; 101: 2023–2027.

[23] Feng J, Liu J, Zhang X, Zhang L, Jiang J, Nolta J, *et al*. Guided Migration of Neural Stem Cells Derived from Human Embry-

onic Stem Cells by an Electric Field. Stem Cells. 2012; 30: 349–355.
[24] Wu D, Ma X, Lin F. DC Electric Fields Direct Breast Cancer Cell Migration, Induce EGFR Polarization, and Increase the Intracellular Level of Calcium Ions. Cell Biochemistry and Biophysics. 2013; 67: 1115–1125.
[25] Li L, El-Hayek YH, Liu B, Chen Y, Gomez E, Wu X, *et al*. Direct-Current Electrical Field Guides Neuronal Stem/Progenitor Cell Migration. Stem Cells. 2008; 26: 2193–2200.
[26] Yao L, Shanley L, McCaig C, Zhao M. Small applied electric fields guide migration of hippocampal neurons. Journal of Cellular Physiology. 2008; 216: 527–535.
[27] Guo A, Song B, Reid B, Gu Y, Forrester JV, Jahoda CAB, *et al*. Effects of Physiological Electric Fields on Migration of Human Dermal Fibroblasts. Journal of Investigative Dermatology. 2010; 130: 2320–2327.
[28] Chang F, Minc N. Electrochemical Control of Cell and Tissue Polarity. Annual Review of Cell and Developmental Biology. 2014; 30: 317–336.
[29] Zhao M, Pu J, Forrester JV, McCaig CD. Membrane lipids, EGF receptors, and intracellular signals colocalize and are polarized in epithelial cells moving directionally in a physiological electric field. FASEB Journal. 2002; 16: 857–859.
[30] Özkucur N, Perike S, Sharma P, Funk RH. Persistent directional cell migration requires ion transport proteins as direction sensors and membrane potential differences in order to maintain directedness. BMC Cell Biology. 2011; 12: 4.
[31] Zhao X, Guan J. Focal adhesion kinase and its signaling pathways in cell migration and angiogenesis. Advanced Drug Delivery Reviews. 2011; 63: 610–615.
[32] Zhang HL, Peng HB. Mechanism of acetylcholine receptor cluster formation induced by DC electric field. PLoS ONE. 2011; 6: e26805.
[33] Fukata M, Nakagawa M, Kaibuchi K. Roles of Rho-family GTPases in cell polarisation and directional migration. Current Opinion in Cell Biology. 2003; 15: 590–597.
[34] Li L, Gu W, Du J, Reid B, Deng X, Liu Z, *et al*. Electric fields guide migration of epidermal stem cells and promote skin wound healing. Wound Repair Regen. 2012; 20: 840–851.
[35] Özkucur N, Song B, Bola S, Zhang L, Reid B, Fu G, *et al*. NHE3 phosphorylation via PKCη marks the polarity and orientation of directionally migrating cells. Cellular and Molecular Life Sciences. 2014; 71: 4653–4663.
[36] Perike S, Özkucur N, Sharma P, Staroske W, Bläsche R, Barth K, *et al*. Phospho-NHE3 forms membrane patches and interacts with beta-actin to sense and maintain constant direction during cell migration. Experimental Cell Research. 2014; 324: 13–29.
[37] Mycielska ME, Djamgoz MBA. Cellular mechanisms of direct-current electric field effects: galvanotaxis and metastatic disease. Journal of Cell Science. 2004; 117: 1631–1639.
[38] Sgarbi G, Baracca A, Lenaz G, Valentino Lucia M, Carelli V, Solaini G. Inefficient coupling between proton transport and ATP synthesis may be the pathogenic mechanism for NARP and Leigh syndrome resulting from the T8993G mutation in mtDNA. Biochemical Journal. 2006; 395: 493–500.
[39] Tan E, Ding X, Saadi A, Agarwal N, Naash MI, Al-Ubaidi MR. Expression of Cone-Photoreceptor–Specific Antigens in a Cell Line Derived from Retinal Tumors in Transgenic Mice. Investigative Opthalmology & Visual Science. 2004; 45: 764.
[40] Wu TD, Nacu S. Fast and SNP-tolerant detection of complex variants and splicing in short reads. Bioinformatics. 2010; 26: 873–881.
[41] Liao Y, Smyth GK, Shi W. Feature Counts: an efficient general purpose program for assigning sequence reads to genomic features. Bioinformatics. 2014; 30: 923–930.
[42] Love MI, Huber W, Anders S. Moderated estimation of fold change and dispersion for RNA-seq data with DESeq2. Genome Biology. 2014; 15: 550.
[43] Benjamini Y, Hochberg Y. Controlling the False Discovery Rate: a Practical and Powerful Approach to Multiple Testing. Journal of the Royal Statistical Society: Series B (Methodological). 1995; 57: 289–300
[44] Li R, Gundersen GG. Beyond polymer polarity: how the cytoskeleton builds a polarized cell. Nature Reviews Molecular Cell Biology. 2008; 9: 860–873.
[45] Guo X, Jiang X, Ren X, Sun H, Zhang D, Zhang Q, *et al*. The Galvanotactic Migration of Keratinocytes is Enhanced by Hypoxic Preconditioning. Scientific Reports. 2015; 5: 10289.
[46] Funk RHW, Monsees T, Özkucur N. Electromagnetic effects – from cell biology to medicine. Progress in Histochemistry and Cytochemistry. 2009; 43: 177–264.
[47] Djamgoz MBA, Mycielska M, Madeja Z, Fraser SP, Korohoda W. Directional movement of rat prostate cancer cells in direct-current electric field: involvement of voltagegated Na+ channel activity. Journal of Cell Science. 2001; 114: 2697–2705.
[48] Gundersen G, Worman H. Nuclear Positioning. Cell. 2013; 152: 1376–1389.
[49] Magdalena J, Millard TH, Machesky LM. Microtubule involvement in NIH 3T3 Golgi and MTOC polarity establishment. Journal of Cell Science. 2003; 116: 743–756.
[50] Magdalena J, Millard TH, Etienne-Manneville S, Launay S, Warwick HK, Machesky LM. Involvement of the Arp2/3 Complex and Scar2 in Golgi Polarity in Scratch Wound Models. Molecular Biology of the Cell. 2003; 14: 670–684.
[51] Pouthas F, Girard P, Lecaudey V, Ly TBN, Gilmour D, Boulin C, *et al*. In migrating cells, the Golgi complex and the position of the centrosome depend on geometrical constraints of the substratum. Journal of Cell Science. 2008; 121: 2406–2414.
[52] Sato MJ, Kuwayama H, van Egmond WN, Takayama AL, Takagi H, van Haastert PJ, *et al*. Switching direction in electric-signal-induced cell migration by cyclic guanosine monophosphate and phosphatidylinositol signaling. Proceedings of the National Academy of Sciences of the United States of America. 2009; 106: 6667–6672.
[53] Vallenius T. Actin stress fibre subtypes in mesenchymal-migrating cells. Open Biology. 2013; 3: 130001.
[54] Etienne-Manneville S. Microtubules in Cell Migration. Annual Review of Cell and Developmental Biology. 2013; 29: 471–499.
[55] Kaverina I, Straube A. Regulation of cell migration by dynamic microtubules. Seminars in Cell & Developmental Biology. 2011; 22: 968–974.
[56] Wittmann T, Bokoch GM, Waterman-Storer CM. Regulation of leading edge microtubule and actin dynamics downstream of Rac1. Journal of Cell Biology. 2003; 161: 845–851.
[57] Etienne-Manneville S. Actin and Microtubules in Cell Motility: which one is in Control? Traffic. 2004; 5: 470–477.
[58] Gomes ER, Jani S, Gundersen GG. Nuclear Movement Regulated by Cdc42, MRCK, Myosin, and Actin Flow Establishes MTOC Polarization in Migrating Cells. Cell. 2005; 121: 451–463.
[59] Petrie RJ, Doyle AD, Yamada KM. Random versus directionally persistent cell migration. Nature Reviews Molecular Cell Biology. 2009; 10: 538–549.
[60] Dugina V, Alieva I, Khromova N, Kireev I, Gunning PW, Kopnin P. Interaction of microtubules with the actin cytoskeleton via cross-talk of EB1-containing +TIPs and γ-actin in epithelial cells. Oncotarget. 2016; 7: 72699–72715.
[61] Nakano A, Kato H, Watanabe T, Min KD, Yamazaki S, Asano Y, *et al*. AMPK controls the speed of microtubule polymerization and directional cell migration through CLIP-170 phosphorylation. Nature Cell Biology. 2010; 12: 583–590.

[62] Ridley AJ. Life at the Leading Edge. Cell. 2011; 145: 1012–1022.
[63] Pu J, Zhao M. Golgi polarization in a strong electric field. Journal of Cell Science. 2005; 118: 1117–1128.
[64] Kim MS, Lee MH, Kwon B, Koo M, Seon GM, Park J. Golgi polarization plays a role in the directional migration of neonatal dermal fibroblasts induced by the direct current electric fields. Biochemical and Biophysical Research Communications. 2015; 460: 255–260.
[65] Bisel B, Wang Y, Wei J, Xiang Y, Tang D, Miron-Mendoza M, *et al*. ERK regulates Golgi and centrosome orientation towards the leading edge through GRASP65. Journal of Cell Biology. 2008; 182: 837–843.
[66] Yadav S, Puri S, Linstedt AD. A Primary Role for Golgi Positioning in Directed Secretion, Cell Polarity, and Wound Healing. Molecular Biology of the Cell. 2009; 20: 1728–1736.
[67] Ravichandran Y, Goud B, Manneville JB. The Golgi apparatus and cell polarity: Roles of the cytoskeleton, the Golgi matrix, and Golgi membranes. Current Opinion in Cell Biology. 2020; 62: 104–113.
[68] Xing M, Peterman MC, Davis RL, Oegema K, Shiau AK, Field SJ. GOLPH3 drives cell migration by promoting Golgi reorientation and directional trafficking to the leading edge. Molecular Biology of the Cell. 2016; 27: 3828–3840.
[69] Yun J, Finkel T. Mitohormesis. Cell Metabolism. 2014; 19: 757–766.
[70] Raefsky SM, Mattson MP. Adaptive responses of neuronal mitochondria to bioenergetic challenges: Roles in neuroplasticity and disease resistance. Free Radical Biology and Medicine. 2017; 102: 203–216.
[71] Castelli V, Benedetti E, Antonosante A, Catanesi M, Pitari G, Ippoliti R, *et al*. Neuronal Cells Rearrangement During Aging and Neurodegenerative Disease: Metabolism, Oxidative Stress and Organelles Dynamic. Frontiers in Molecular Neuroscience. 2019; 12: 132.
[72] Onuma EK, Hui SW. Electric field-directed cell shape changes, displacement, and cytoskeletal reorganization are calcium dependent. Journal of Cell Biology. 1988; 106: 2067–2075.
[73] Borys P. The role of passive calcium influx through the cell membrane in galvanotaxis. Cellular and Molecular Biology Letters. 2013; 18: 187–199.
[74] Bravo R, Vicencio JM, Parra V, Troncoso R, Munoz JP, Bui M, *et al*. Increased ER–mitochondrial coupling promotes mitochondrial respiration and bioenergetics during early phases of ER stress. Journal of Cell Science. 2011; 124: 2143–2152.
[75] Green DR, Wang R. Calcium and Energy: Making the Cake and Eating it too? Cell. 2010; 142: 200–202.
[76] Zanotelli MR, Rahman-Zaman A, VanderBurgh JA, Taufalele PV, Jain A, Erickson D, *et al*. Energetic costs regulated by cell mechanics and confinement are predictive of migration path during decision-making. Nature Communications. 2019; 10: 4185.
[77] Fang WB, Jokar I, Zou A, Lambert D, Dendukuri P, Cheng N. CCL2/CCR2 Chemokine Signaling Coordinates Survival and Motility of Breast Cancer Cells through Smad3 Protein- and p42/44 Mitogen-activated Protein Kinase (MAPK)-dependent Mechanisms. Journal of Biological Chemistry. 2012; 287: 36593–36608.
[78] Saha M, Mitsuhashi S, Kang P. Identification and Characterization of Disease Mechanisms in MEGF10 Myopathy. FASEB Journal. 2015; 29: 1038.1031.
[79] Kawahara E, Maenaka S, Shimada E, Nishimura Y, Sakurai H. Dynamic Regulation of Extracellular Signal-Regulated Kinase (ERK) by Protein Phosphatase 2A Regulatory Subunit B56?1 in Nuclei Induces Cell Migration. PLoS ONE. 2013; 8: e63729.
[80] Vora P, Pillai P, Mustapha J, Kowal C, Shaffer S, Bose R, *et al*. CXCL1 regulation of oligodendrocyte progenitor cell migration is independent of calcium signaling. Experimental Neurology. 2012; 236: 259–267.
[81] Hägglund MGA, Sreedharan S, Nilsson VCO, Shaik JHA, Almkvist IM, Bäcklin S, *et al*. Identification of SLC38a7 (SNAT7) Protein as a Glutamine Transporter Expressed in Neurons. Journal of Biological Chemistry. 2011; 286: 20500–20511.
[82] Pan C-J, Chen S-Y, Jun HS, Lin SR, Mansfield BC, Chou JY. SLC37A1 and SLC37A2 Are Phosphate-Linked, Glucose-6-Phosphate Antiporters. PLoS ONE. 2011; 6: e23157.
[83] Moreno-Carralero M-I, Muñoz-Muñoz J-A, Cuadrado-Grande N, López-Rodríguez R, José Hernández-Alfaro M, del-Castillo-Rueda A, *et al*. A novel mutation in the SLC40A1 gene associated with reduced iron export in vitro. American Journal of Hematology. 2014; 89: 689–694.